ACS APPLIED MATERIALS & INTERFACES

Research Article

www.acsami.org

Structural and Nanomechanical Properties of Paperboard Coatings Studied by Peak Force Tapping Atomic Force Microscopy

Majid Sababi,[†] John Kettle,[‡] Hille Rautkoski,[‡] Per M. Claesson,[†,§] and Esben Thormann*[,†]

[†]KTH Royal Institute of Technology, School of Chemical Science and Engineering, Department of Chemistry, Surface and Corrosion Science, Drottning Kristinas väg 51, SE-100 44 Stockholm, Sweden

[‡]VTT Technical Research Centre of Finland, Functional Fibre Products, Biologinkuja 7, Espoo, PL 1000, FI-02044 VTT, Finland

[§]YKI Institute of Surface Chemistry, P.O. Box 5707, SE-114 86 Stockholm, Sweden

ABSTRACT: Paper coating formulations containing starch, latex, and clay were applied to paperboard and have been investigated by scanning electron microscopy and Peak Force tapping atomic force microscopy. A special focus has been on the measurement of the variation of the surface topography and surface material properties with a nanometer scaled spatial resolution. The effects of coating composition and drying conditions were investigated. It is concluded that the air-coating interface of the coating is dominated by close-packed latex particles embedded in a starch matrix and that the spatial distribution of the different components in the coating can be identified due to their variation in material properties. Drying the coating at an elevated temperature compared to room temperature changes the surface morphology and the surface material properties due to partial film formation of latex. However, it is evident that the chosen elevated drying temperature and exposure time is insufficient to ensure complete film formation of the latex which in an end application will be needed.

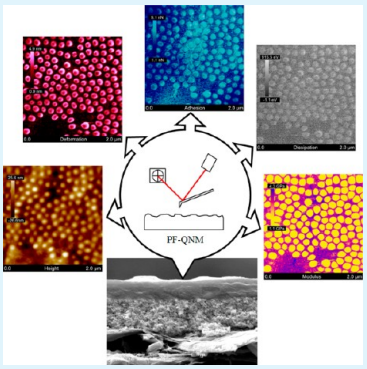

KEYWORDS: *atomic force microscopy, material properties, nanocomposites, coating, paperboard, topography*

INTRODUCTION

Fiber-based materials are widely used in the packaging world to protect their contents against physical and chemical damage, contamination, humidity, and light.[1] Normally, the diverse functionalities of paperboard are obtained through the application of coating layers containing a range of selected binders and pigments, applied in aqueous suspension at high speed. Examples of such coating additives are natural or synthetic binders[2−8] and pigments such as calcium carbonate, kaolin, or talc.[9−11] In this study, we have examined paperboards that have been topcoated with simple coating formulations which consist of different relative amounts of starch, SB latex, and clay. The paperboard was selected as the material to be used in these studies in order to provide a substrate that minimized the penetration of the applied coating formulation.

General mechanical properties of the paperboards such as strength and foldability can be evaluated with conventional mechanical tests like indentation, dynamic mechanical analysis, and tensile testing.[12−14] These types of tests provide valuable information about the overall lateral mechanical properties of the paperboards, but there are other properties, for example, printability and resistance, toward absorption of moisture which are directly related to the chemical and mechanical properties of paperboard coatings.[15]

There are a number of studies devoted to the compressive characteristics of papers.[16−18] In such studies, properties like modulus or compressibility are evaluated by measuring the change in thickness as a function of normal load and using an exponential fitting to the stress−strain relationship in order to yield the parameter related to the elastic modulus.[2,16,17] Although these techniques are straightforward to apply, they measure the properties of the entire paperboard, including both bulk paper properties and the coating properties, and these properties are in addition average values with respect to lateral variations. However, it is more complex to examine the spatial variation in mechanical properties on a similar length scale to the particle additives in the size range of nanometer to micrometer scale.

Peak Force tapping is a relatively new imaging mode for atomic force microscopy (AFM)[19,20] which allows analysis of mechanical properties in the vertical direction with nanometer scale lateral resolution, and it is thus possible to map spatial variations in material properties across the interface of a structured surface layer, like that formed by a coating. In this work, the mechanical properties of paperboard coatings with different compositions and dried under different conditions were investigated with Peak Force tapping AFM and electron scanning microscopy (SEM).

MATERIAL AND METHODS

Materials. Fully coated CTMP paperboards with a grammage of 200 g/m^2 and a thickness of 295 μm from Stora Enso (Helsinki, Finland) were used as the substrate in this work. The composition and

Received: July 24, 2012
Accepted: September 13, 2012
Published: September 13, 2012

   dx.doi.org/10.1021/am301439k | ACS Appl. Mater. Interfaces 2012, 4, 5534−5541

thickness details of the already applied coating layers, which we in this study refer to as the "triple coating", were not provided.

To achieve a simple coating structure with a known composition, three different topcoatings consisting of a pure starch, a mixture of starch and latex, and a mixture of starch, latex, and clay were applied to the commercial paperboard samples. These samples were further dried at two different conditions giving a total number of six coated paperboard samples in addition to an uncoated reference sample. The coating matrix is based on a combination of starch (Raisamyl 01511, Chemigate Oy Lapua, Lapua Finland), SB latex (DL 966, Styron Suomi Oy, Helsinki, Finland), and clay (Capim SP, Imerys Ltd., Paris, France). The SB latex was in the form of monodisperse particles with a diameter of 145 nm and a glass transition temperature of T_g = 18 °C. Capim SP clay has a particle size distribution that is 98% by weight finer than 2 μm.

The coatings were applied by an Erichsen rod applicator at an application speed of 24 mm/s speed (80 μm rod for starch coatings and 50 μm rod for the other coatings). The coatings were dried either at room temperature or at 105 °C for 5 min. Nominal compositions of these coatings, given as relative amounts of dry mass, are provided in Table 1. In the following, we will refer to these six different samples with a name based on their composition and drying condition (see Table 1).

Table 1. Composition of Paperboard Samples Used in This Study Given as Relative Amount of Dry Mass

sample	drying condition	starch	SB latex	clay
Starch100-HT	105 °C, 5 min	100	0	0
Starch50-Latex50-HT	105 °C, 5 min	50	50	0
Starch50-Latex50-Clay30-HT	105 °C, 5 min	50	50	30
Starch100-RT	room temperature	100	0	0
Starch50-Latex50-RT	room temperature	50	50	0
Starch50-Latex50-Clay30-RT	room temperature	50	50	30

Methods. *Scanning Electron Microscopy.* A scanning electron microscope (SEM) (FEI XL30 ESEM) was used to investigate the bulk topcoating morphology. Measurements were performed in a mixture of secondary and backscatter electron mode (90% SE plus 10% BSE) with 25 keV accelerating voltage in order to obtain information on both topographical and material properties. Samples were cross-sectioned to investigate coating morphology at different depths. For cross-sectioning, the paperboards were immersed in liquid nitrogen to make them brittle and then snapped to break them apart. Next, the cross sections were gold sputtered for around 10 min, to create an approximately 5 nm gold layer in order to make the surface conductive.

AFM Imaging. Nanometer scale lateral resolution images of surface topography and surface material properties were obtained using an atomic force microscope (AFM) (Multimode, Nanoscope V, Bruker) operating in Peak Force tapping mode using rectangular silicon cantilevers (NSC15, Mikromasch). This cantilever is backside coated with a reflective aluminum layer and has an n-type silicon etched (phosphorus doped) tip with a nominal radius of 10 nm, and the total tip height is on the order of 21−25 μm.

Peak Force tapping is a relatively new imaging mode which allows imaging with a controlled feedback force[21] and simultaneously provides access to quantitative mapping of surface material properties.[22−24] Briefly, the surface position is modulated by a sine wave with amplitude of approximately 150 nm and a frequency of 2 kHz. During each period of oscillation, the surface is moved into contact with the AFM tip and the feedback electronics adjust the averaged surface position such that the maximum cantilever deflection (the peak force) equals a predetermined set point value. By calibration of the optical lever sensitivity[25] and the cantilever spring constant[26,27] (45.2 N/m for the cantilever used in this study), the information about cantilever deflection and piezo position can be converted to force vs distance curves describing the tip−sample interaction during approach and separation (see Figure 1). From such a force curve, one can read the surface deformation due to the tip−sample interaction, the maximum

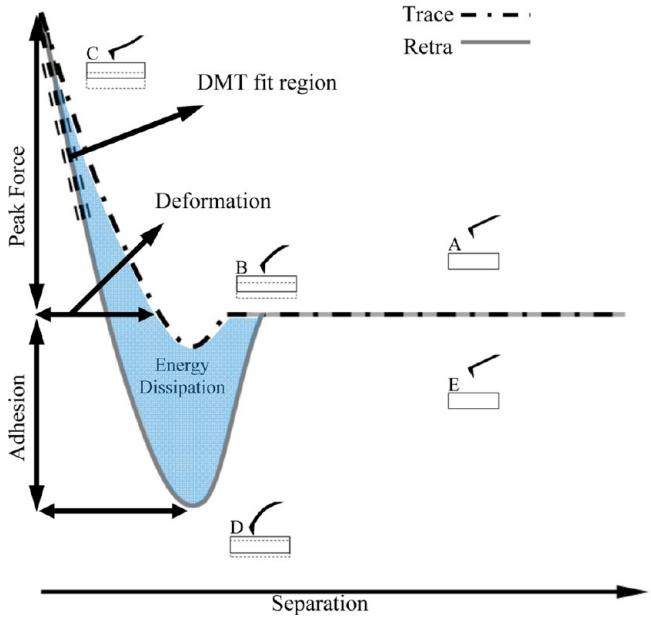

Figure 1. Schematic illustration of a force-separation curve generated during one cycle in Peak Force AFM. At position (A), the tip is out of contact and no force is detected. At position (B), the tip is dragged into contact by an attractive force. At position (C), the sample is deformed by a positive applied load. At position (D), the tip and sample are held together at negative load by adhesion. At position (E), it is again brought out of contact and the cycle is completed. From the force-separation curve, sample deformation, tip−sample adhesion, energy dissipation, and elastic modulus are determined.

adhesion force between the tip and the sample, and the amount of energy that is dissipated during the interaction. In addition, one can determine the elastic modulus of the sample by fitting the Derjaguin-Muller-Toporov (DMT) model[28,29] to the part of the force curve where the sample and tip are in contact:

$$F = \frac{4}{3}E^*\sqrt{Rd^3} + F_{adh}$$

Here, F is the force, E^* is the effective elastic modulus, R is the tip radius, d is the deformation value at a given force, and F_{adh} is the maximum adhesion force. In this study, we have determined the tip radius by an indirect method where the radius was adjusted to achieve the correct value of a sample with known elastic modulus (polystyrene, E = 2.7 GPa). By this method, the tip radius was estimated to be 11 nm, which is in good agreement with the nominal value of 10 nm provided by the manufacture. In Peak Force tapping, a new set of force versus separation curves are obtained during each period of oscillation (every 0.5 ms), and the values of deformation, adhesion, dissipation, and elastic modulus is extracted in real time. This means that, as the sample is scanned, images showing the variation in these properties are obtained simultaneously with the topographical information.

Image analysis was performed with the Nanoscope Analysis v.120 software (Bruker). The topography images were subjected to a second order polynomial flattening algorithm to correct for surface tilt and bow effects. Adhesion images obtained at 10 × 10 μm^2 scan size were subjected to high-pass Gaussian filter with a filter size of 2.2 μm in order to remove noise induced by optical interference in the detection system which are leading to minor variations in the baseline values of the force curves. The weak stripes seen in Figure 4A-IV,A-V are also an effect of optical interference. However, for these and the remaining images, only the color scales were adjusted in order to optimize the image contrast. Roughness analysis was performed for all samples for

both 2 × 2 and 10 × 10 μm^2 images, and the results of this analysis are collected in Table 2.

Table 2. Calculated Roughness Values for Paperboard Samples

	10 μm		2 μm	
sample	R_q	R_a	R_q	R_a
Uncoated-RT	69.2	55.6	36.2	28.2
Starch100-HT	25.6	22.1	3.13	3.93
Starch50-Latex50-HT	17.2	13.8	3.07	2.34
Starch50-Latex50-Clay30-HT	22.1	17.1	5.24	3.74
Starch100-RT	29.7	23.7	5.04	4.04
Starch50-Latex50-RT	18.4	14.3	7.12	5.68
Starch50-Latex50-Clay30-RT	41.5	31.5	9.12	7.10

RESULTS AND DISCUSSIONS

Scanning Electron Microscope Investigation. Figure 2A shows a low magnification SEM image of the cross-section of a paperboard. As described in the Methods section, the paperboard consists of the bulk paperboard material, an industrially applied triple coating, and a laboratory applied top coating with a dried thickness of around 5−10 μm which in our case consists of pure starch, starch/latex, or starch/latex/clay. Figure 2B−D shows images of different magnifications of these three top coatings. Figure 2B,C illustrates the coatings containing pure starch (Starch100-HT) and starch and latex (Starch50-Latex50-HT) which on this length scale appears smooth and homogeneous in the structure. In contrast, Figure 2D showing the coating containing starch, latex, and clay (Starch50-Latex50-Clay30-HT) appears different. The clay particles have the form of thin sheets with lateral dimensions of a few micrometers. Such particles are easily recognized in the SEM image due to their high backscatter intensity, and these particles appear to be equally distributed in the bulk of the coating. In the following, we will be focusing on the interfacial properties of the top coating and not on the bulk structure of the underlying coating.

Peak Force Tapping Imaging. *Nanomechnical Mapping of Composite Coatings.* Large scale Peak Force tapping mode images of untreated paperboard and paperboards with coatings dried at room temperature (Starch100-RT, Starch50-Latex50-RT, and Starch50-Latex50-Clay30-RT) are shown in Figures 3 and 4. The Starch100-RT coating (Figure 4A-I−A-V) appears uniform with a surface roughness of R_q = 29.7 nm and an average elastic modulus of 3.3 GPa. Since Starch100-RT is a single component coating, no large local variation is observed in the deformation, dissipation, adhesion, and elastic modulus images. In comparison to the starch coating, it is observed from Figure 3 that the as received triple coating is much rougher (R_q = 69.2 nm) while the average elastic modulus is slightly lower (1.5 GPa).

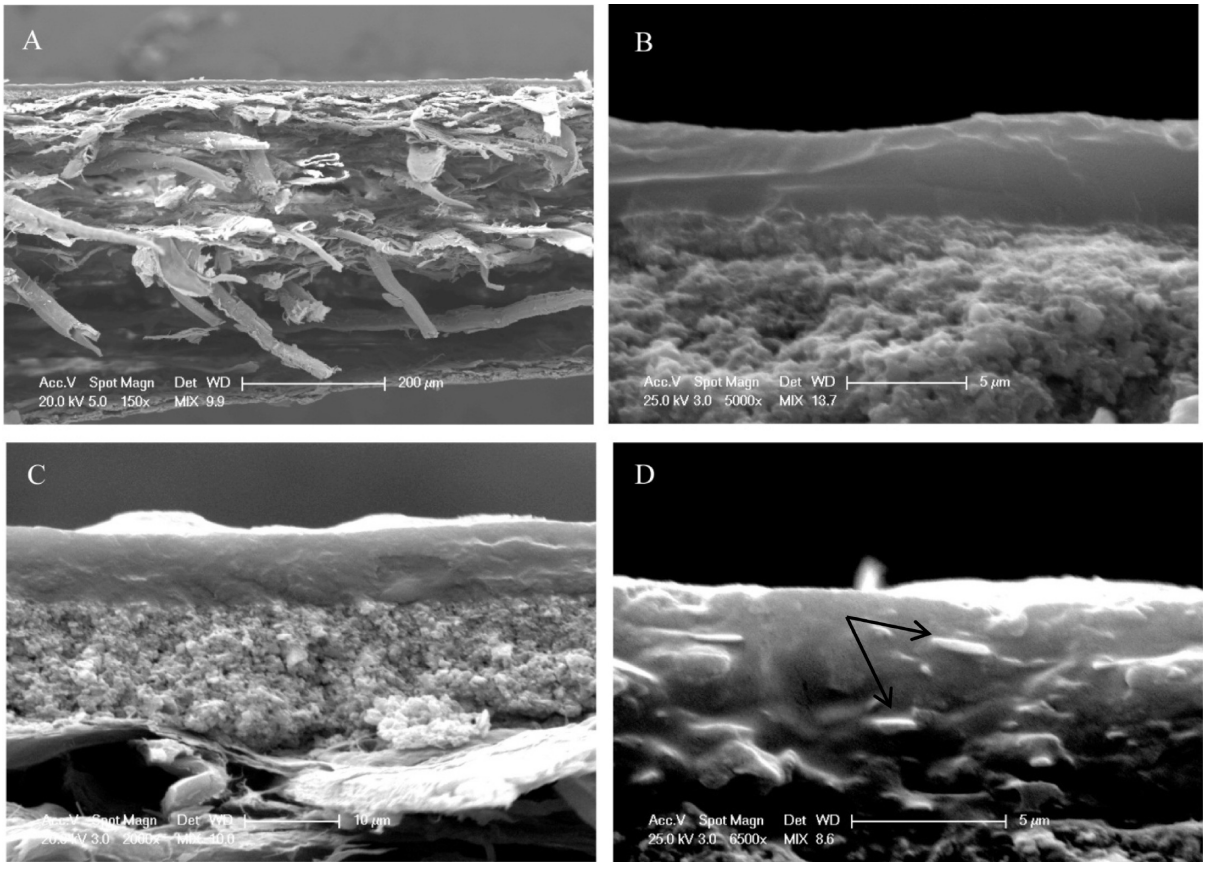

Figure 2. Cross-section SEM images of paperboard and paperboard coatings showing the topographical structure. (A) Overview SEM image (150×) of the paperboard, triple coating and top coating (Starch50-Latex50-HT). High resolution SEM image of (B) Starch100-HT (5000×), (C) Starch50-Latex50-HT (2000×), and (D) Starch50-Latex50-Clay30-HT (6500×). The arrows in (D) are highlighting the location of two larger clay particles inside the coating layer.

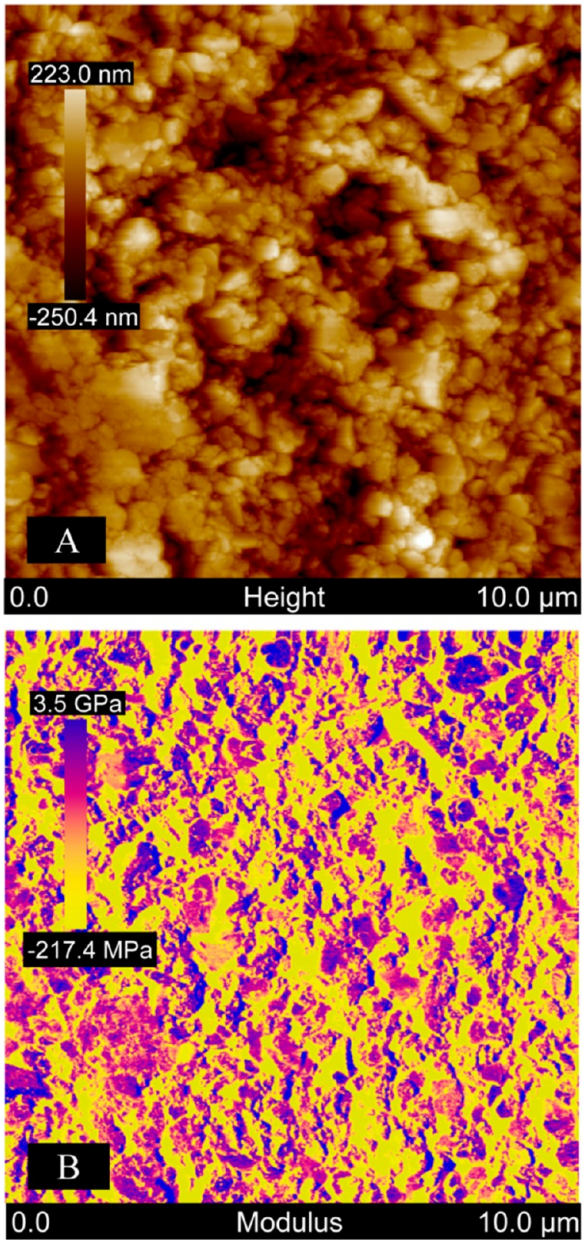

Figure 3. Peak Force tapping AFM image of paperboard with as received triple coating: (A) height and (B) elastic modulus (average elastic modulus = 1.5 ± 0.04 GPa).

The effect of adding latex to the coating (Starch50-Latex50-RT) can be observed in Figure 4B-I–B-V. In the height image (Figure 4B-I), the latex is seen to result in a dot pattern morphology corresponding to the presence of a layer of latex particles at the interface. It is evident that the latex particles are packed closely together except in some areas where some of the particles are absent from the surface. The presence of latex particles lead to a slight decrease in the surface roughness to R_q = 18.4 nm compared to R_q= 29.7 nm for the pure starch coating. We believe that this decrease in roughness is because of their tendency to form a closed-packed layer at the interface, ensuring a smooth and homogeneous coating surface on a large length scale although they introduce more height variations on a short length scale. The latex particles and their packing geometry are even more clearly seen in the deformation, energy dissipation, adhesion, and elastic modulus images (Figure 4B-II–B-V) which are displaying two distinct phases. From the color codes in these images, the latex particles are observed to have higher deformation, higher energy dissipation, higher adhesion, and lower elastic modulus values compared to the surrounding starch matrix.

Figure 4C-I–C-V displays the height, deformation, energy dissipation, adhesion, and elastic modulus images of the Starch50-Latex50-Clay30-RT coating. From the SEM images in Figure 2D, we know that the clay particles are found as flakes with plate dimensions of a few micrometers and thickness on the order of 100 nm. A few of these structures are also identified in the height image (see arrows in Figure 4C-I), and these flake-like structures further display a smaller deformation (Figure 4C-II) and higher elastic modulus (Figure 4C-V) than both the latex particles and the starch matrix. This is expected since the mineral is naturally harder than the polymeric material. This also illustrates how Peak Force imaging can be used to distinguish the different components in a coating layer. It is apparent that the number of clay particles observed at the interface does not represent the bulk concentration of clay. This result illustrates that even in the composite coating layer the interfacial region is dominated by the latex particles in this type of formulation. We suggest this is because the latex particles are more surface active in a water-based coating and that these particles thus dominate at the coating–air interface during the drying process which is in agreement with previous studies of latex migration during coating consolidation.[30,31]

Since the large scan areas, as shown in Figure 4, reveal that the interfacial region is dominated by starch and latex, even for coatings with a relatively high bulk clay concentration, we will in the following focus on the surface mechanical properties of starch and latex. Figure 5A-I–A-V displays 2 × 2 μm^2 images of the Starch50-Latex50-RT coating. These high resolution images are presented together with line scans over three representative adjacent latex particles which provide further detailed information about how the latex particles are packing at the interface and how the mechanical properties are varying at the nanometer scale. It is evident here that the latex particles are packed in a near hexagonal pattern. However, at first, it appears as if the particles are not closed-packed since material with starch-like properties is spanning the surface area between neighboring particles. However, the peak to peak distance corresponding to the distance between two particle centers is found to be approximately 150 nm and thus very close to the actually size of the latex particles. Further, a closer inspection of the height to width ratio of the spherical cap, evaluated from the line scan analysis, reveals that starch is found between the particles because only a small fraction of the latex particles is sticking out of the starch matrix (like an iceberg at the air–water interface). Figure 6 illustrates how the height to width ratio fits with a layer of closed-packed particle with an approximate diameter of 150 nm, where only about 10–15 nm of the particles is above the starch matrix.

The line scan analysis also reveals how the surface material properties are varying quantitatively. The deformation, adhesion, dissipation, and elastic modulus images show almost uniform material properties across a particle but distinctly different values between the particles and the matrix with a surface elastic modulus of approximately 2 and 3.5 GPa of the latex and starch, respectively (Table 3). The fact that the measured deformation, adhesion, and elastic modulus are almost constant over the cross-section of a particle also illustrates that the measured values apparently are not

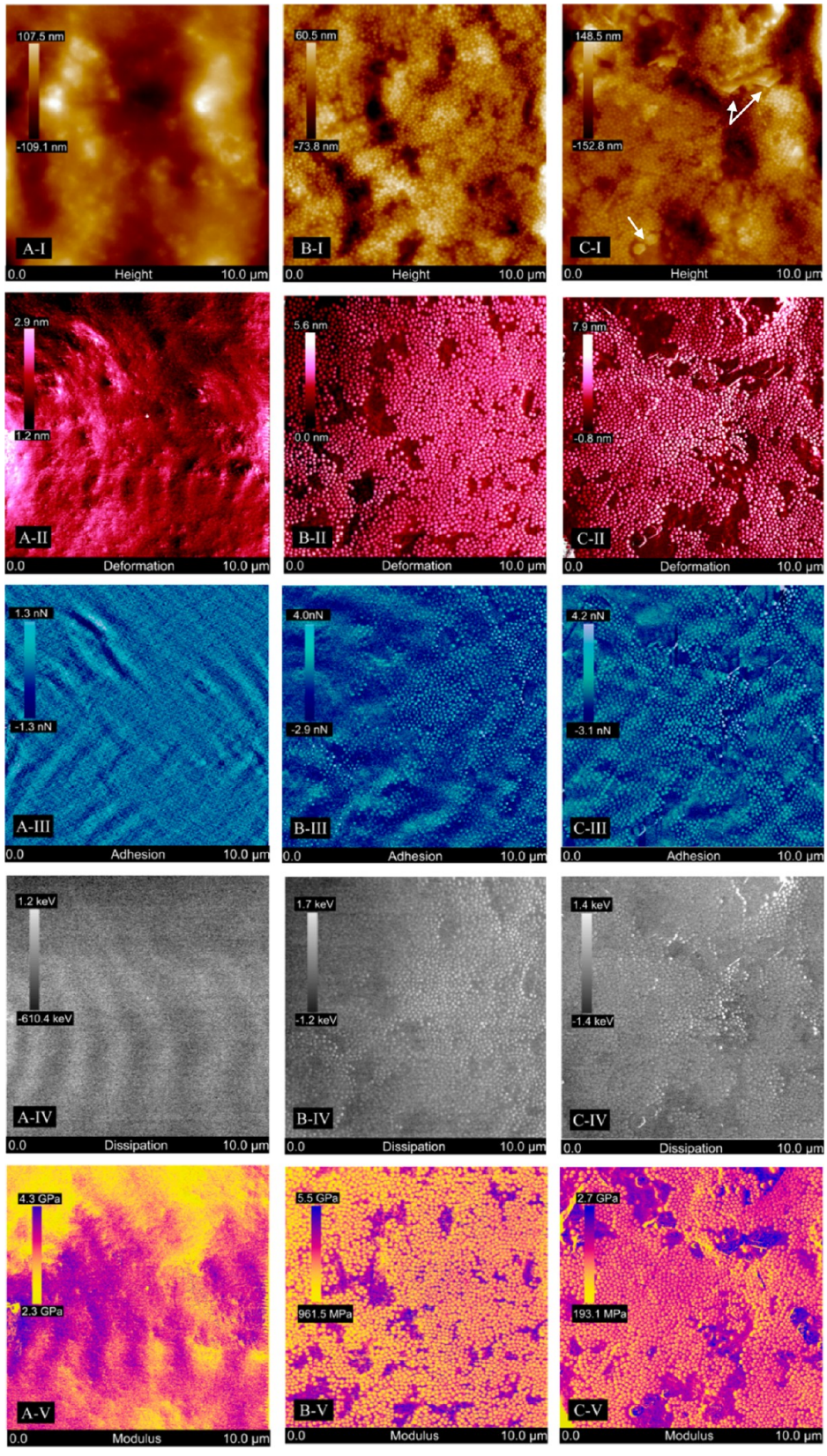

Figure 4. Peak Force tapping AFM images of: Starch100-RT, (A-I) height, (A-II) deformation, (A-III) adhesion, (A-IV) dissipation, and (A-V) modulus; Starch50-Latex50-RT, (B-I) height, (B-II) deformation, (B-III) adhesion, (B-IV) dissipation, and (B-V) modulus; Starch50-Latex50-Clay30-RT, (C-I) height, (C-II) deformation, (C-III) adhesion, (C-IV) dissipation, and (C-IV) modulus. The arrows in C-I highlight the positions of some of the clay particles located at the interface.

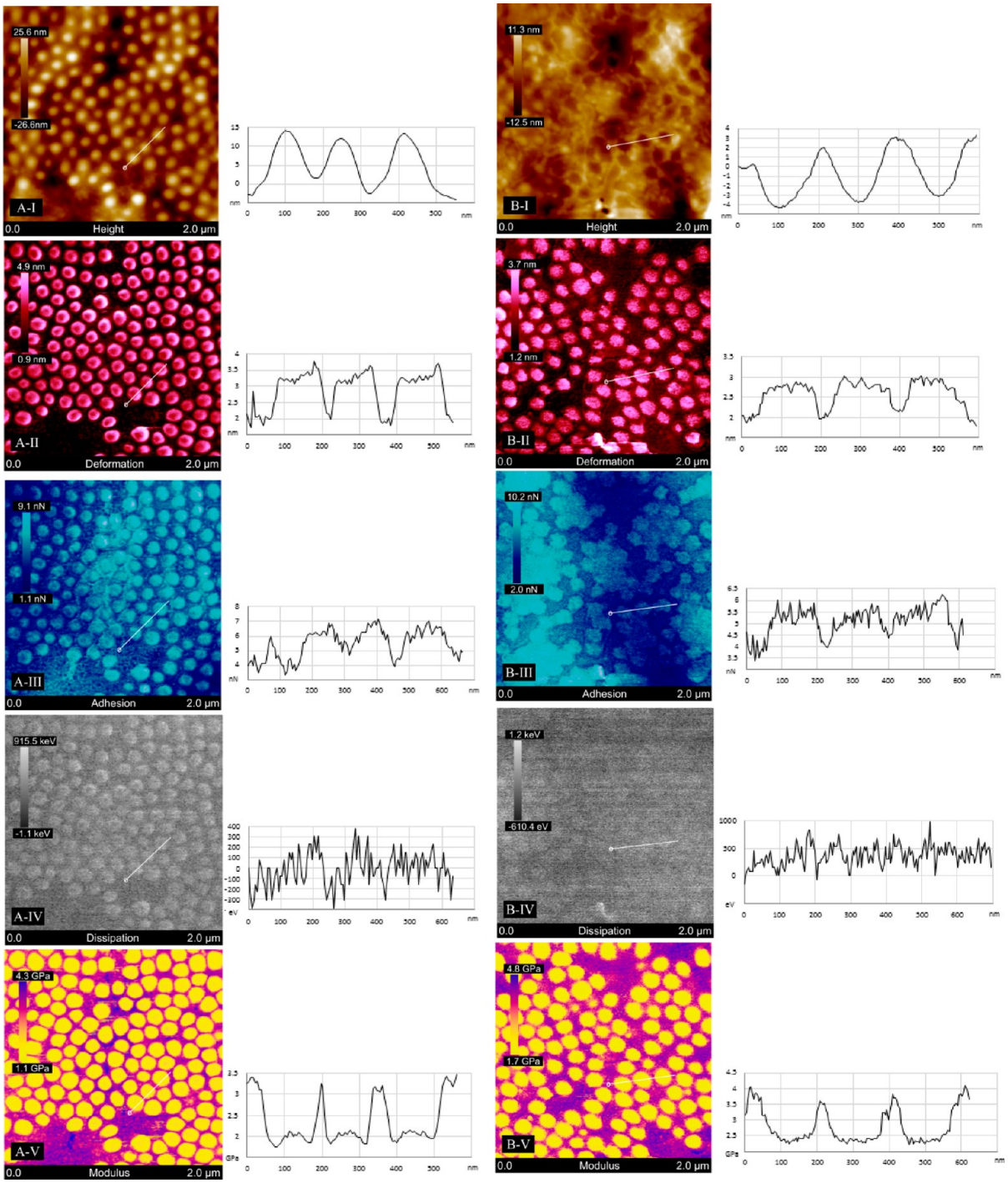

Figure 5. Peak Force tapping AFM images illustrating the effect of drying temperature on mechanical properties, Starch50-Latex50-RT, (A-I) height, (A-II) deformation, (A-III) adhesion, (A-IV) dissipation, and (A-V) modulus; Starch50-Latex50-HT, (B-I) height, (B-II) deformation, (B-III) adhesion, (B-IV) dissipation, and (B-V) modulus.

significantly affected by the local curvature at the point of impact between the AFM-tip and the surface. In Table 2, we have compared average values of the elastic modulus for the three components investigated in this study with values that have previously been reported. The values for starch and latex based on the data from Figures 4C-V and 5A-V,B-V are within the range close to most of the reported values although some variations between the values obtained with different methods are observed. The value for clay based on data from Figure 4C-V is also within the range of most reported values. However, one should always be careful when performing a direct comparison between local values found for different components in a composite material with the bulk value of the pure materials. Surface properties are often different from bulk properties, and the values of latex and clay could be affected by the presence of starch. It should further be noted that the elastic modulus of clay is strongly dependent on both the exact mineral structure and direction of the material deformation with respect to the mineral plane.[32] These are parameters which are not controlled in this study.

dx.doi.org/10.1021/am301439k | ACS Appl. Mater. Interfaces 2012, 4, 5534−5541

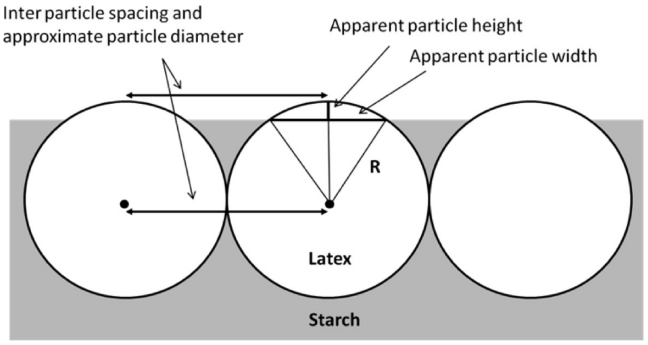

Figure 6. Schematic illustration of latex particles in a starch matrix showing how latex particles are packed at the interface of the paperboard coating when dried at room temperature.

Table 3. Comparison between the Elastic Modulus (in Units of GPa) of Starch, Latex, and Clay Found in This Study Compared to Previously Reported Values

methods	starch	latex	clay
peak force tapping atomic force microscopy	3.5 ± 0.7[a]	2.2 ± 0.5[a]	6.1 ± 1.2[a]
instrumented indentation (IIT)		1.14 ± 0.03[14]	18−178[b,32]
tensile test	1.1−2.2[33]	0.63 ± 0.09[14]	1.80[34]
dynamic mechanical analysis (DMA)		0.48 ± 0.15[14]	
ultrasonic measurements	5 ± 0.05[35]		3−9[c,36]
acoustic measurements			6−12[d,37]
modulated force thermo mechanical analysis (AFAM)			6.2 ± 2.5[e,38]
strain-induced elastic buckling measurements	1.8[39]		

[a]This paper. [b]Muscovite, vermiculite, pyrophyllite, talc, and rectorite. [c]Clay as soil at freeze temperature (−2 to −10 °C). [d]Bulk modulus value (Kaolinite, montmorillonite, and smectite). [e]Kaolinite, dickite, and mica powders.

Effect of High Temperature Drying. In Figure 5B-I−B-V, 2 × 2 μm^2 images are shown of a coating containing starch and latex (Starch50-Latex50-HT) in the same ratio as in the coatings described above. However, as compared to the previous samples, which had been dried at room temperature, these coatings were dried at 105 °C for 5 min. Since this temperature is far above the glass transition temperature of the latex particles (18 °C), the change in drying condition is expected to significantly soften the latex particle and thus to change the structure and the mechanical properties of the coating. First, we note that an elevated temperature leads to a smoother surface with a roughness of R_q = 17.2 nm compared to R_q = 18.4 nm measured for the sampled dried at room temperature (both values based on 10 × 10 μm^2 images; see Table 2). More specific changes are also observed. The height image (Figure 5B-I) shows round objects with approximately the same lateral dimension as those in the coating dried at room temperature (Figure 5A-I). However, while the round objects in the previous case were assigned to latex particles sticking out of the starch matrix, it is noteworthy that these objects now represent spherical surface depressions with a depth of approximately 4 nm. From the height image, it is not possible to predict if these depressions correspond to latex particles that have sunk into the starch matrix or represent imprints in the starch matrix from where the latex was previously present. In the deformation, adhesion, dissipation, and elastic modulus images, the contrast between the depressions and the surrounding matrix is much higher than in the height image, and it is further seen that the surface layer in the surface depressions possess the same mechanical and adhesive properties as the latex particles sticking out of the starch matrix in the case of the coating being dried at room temperature. Thus, the depressions represent latex particles that have sunk into the starch matrix. In the deformation and elastic modulus images (Figure 5B-II−B-V), the round domains still appear separated from each other although the edges are less sharp compared to those in the coating dried at room temperature. However, in the adhesion image and to a minor extent in the dissipation image (Figure 5B-III,B-IV), several of the round domains have clearly fused. We interpret these observations in the following way: During the drying process, the latex particles start to deform and melted latex diffuses into the starch matrix. This means that the overall apparent height of the latex particle is decreased from 10 to 15 nm above the starch matrix to around 4 nm below the starch layer. It is evident from the mechanical and adhesive properties that the surface depressions still consist of latex and not of starch. The more diffuse edges in the deformation and elastic modulus images show that latex and starch indeed have started to mix at elevated temperatures. To understand why the particles appear to be fused in the adhesion images and not in the deformation and elastic modulus images, one has to understand the nature of the tip−sample interactions which is responsible for the contrast in the different images (as described in relation to Figure 1). The deformation image is a direct measure of the sample deformation as the AFM tip is approached and pressed into the sample with a certain applied force. The elastic modulus image is obtained by fitting the DMT model to the deformation curve obtained as the tip is retracted after the initial deformation. Thus, these images are both related to the mechanical properties of the material in the part of the sample which is influenced by the deformation. As a rule of thumb, these quantities will be influenced by the properties of the sample down to a depth that corresponds to approximately twice the indentation depth (2−3 nm in our case). The adhesion image is related to the direct adhesive contact between the sample and the AFM tip and will thus in contrast to the mechanical responses primarily be related to the properties of the topmost surface. With this in mind, we suggest that the different appearance of the adhesion, deformation, and elastic modulus images in Figure 5 reflects different properties at the topmost interface and in the first 4−5 nm of the coating. As the particles have started to melt, a thin latex film has apparently formed between some of the particles. Such a film is easily detected in the adhesion image as described above. However, if the film is on the order of 1 nm or thinner, the measured deformation and elastic modulus will primarily reflect the underlying starch matrix and will thus not give rise to a contrast where the particles appear to have fused.

CONCLUSIONS

In this study, maps with a nanometer scale spatial resolution of surface topography and surface material properties of laboratory coatings applied to triple coated paperboard were obtained by a newly developed AFM technique. It was demonstrated how different components in a coating layer can be distinguished from their different material properties. For composite coatings dried at room temperature, the

interface was observed to be dominated by closed-packed latex particles embedded in a starch matrix, which is suggested to be a consequence of its higher surface activity compared to starch and clay particles. In the paper industry, coatings are normally dried at elevated temperatures to give rise to film formation and thereby enhance the strength properties of the coating. In the present case, coatings dried at 105 °C for 5 min show incomplete film formation. The transition from a system where latex particles are sticking out of the starch matrix to a system where spherical surface depressions of latex are found as well as the diffuse edges of the latex domains show that latex and starch have started to mix at the elevated temperature. However, in order to form defect free barrier layers, our investigation has revealed that the heat treatment used in this laboratory scale experiment is insufficient, and we suggest that this AFM technique can be used to investigate the effectiveness of different coating treatments on a spatial level which is not achievable with any conventional techniques.

AUTHOR INFORMATION

Corresponding Author

*Fax: +46(0)8208284. Tel: +46(0)87909920. E-mail: esben@kth.se.

Author Contributions

The manuscript was written through contributions of all authors. All authors have given approval to the final version of the manuscript.

Notes

The authors declare no competing financial interest.

ACKNOWLEDGMENTS

This work was supported by the SSF program "Microstructure, Corrosion and Friction Control".

REFERENCES

(1) Rhim, J. W.; Kim, J. H. *J. Food Sci.* **2009**, *74*, E105.
(2) Azadi, P.; Nunnari, S.; Farnood, R.; Kortschot, M.; Yan, N. *Prog. Org. Coat.* **2009**, *64*, 356.
(3) El-Saied, H.; Basta, A. H.; Elsayad, S. Y.; Morsy, F. *Polymer* **1995**, *36*, 4267.
(4) Sato, K. *Prog. Org. Coat.* **1976**, *4*, 271.
(5) Shen, J.; Song, Z.; Qian, X.; Yang, F. *Carbohydr. Polym.* **2010**, *81*, 545.
(6) Fardim, P.; Holmbom, B. *Appl. Surf. Sci.* **2005**, *249*, 393.
(7) Park, J.-K.; Kim, J.-K.; Kim, H.-K. *J. Mater. Process. Technol.* **2007**, *186*, 367.
(8) Hubbe, M. A.; Pawlak, J. J.; Koukoulas, A. A. *BioResources* **2008**, *3*, 627.
(9) Bundy, W. M.; Ishley, J. N. *Appl. Clay Sci.* **1991**, *5*, 397.
(10) Preston, J. S.; Elton, N. J.; Husband, J. C.; Dalton, J.; Heard, P. J.; Allen, G. C. *Colloids Surf., A* **2002**, *205*, 183.
(11) Dalton, J. S.; Preston, J. S.; Heard, P. J.; Allen, G. C.; Elton, N. J.; Husband, J. C. *Colloids Surf., A* **2002**, *205*, 199.
(12) Kim, C.-K.; Lim, W.-S.; Lee, Y. K. *J. Ind. Eng. Chem.* **2010**, *16*, 842.
(13) Schuman, T.; Wikström, M.; Rigdahl, M. *Prog. Org. Coat.* **2004**, *51*, 220.
(14) Forster, A. M.; Watson, S.; White, J. *Nanotechnol. Appl. Coat.* **2009**, *1008*, 274.
(15) Lepoutre, P. *Prog. Org. Coat.* **1989**, *17*, 89.
(16) Heikkila, I. *Pap. Puu-Pap. Timber* **1997**, *79*, 186.
(17) Mangin, P. J. *Tappi J.* **1986**, *69*, 90.
(18) Yamauchi, T. *Appita J.* **1989**, *42*, 222.
(19) PittengerB.ErinaN.SuC.Quantitative mechanical property mapping at the nanoscale with PeakForce QNM. Application Note, Veeco Instructions, Inc. http://www.bruker-axs.com/uploads/tx_linkselectorforpdfpool/Quantitative_Mechanical_Property_Mapping_at_the_Nanoscale_with_PeakForce- QNM_AFM_AN128.pdf.
(20) Morsi, S. M.; Pakzad, A.; Amin, A.; Yassar, R. S.; Heiden, P. A. *J. Colloid Interface Sci.* **2011**, *360*, 377.
(21) Bodvik, R.; Thormann, E.; Karlson, L.; Claesson, P. M. *Phys. Chem. Chem. Phys.* **2011**, *13*, 4260.
(22) Rico, F.; Su, C.; Scheuring, S. *Nano Lett.* **2011**, *11*, 3983.
(23) Foster, B. *Am. Lab.* **2012**, *44*, 24.
(24) Sweers, K.; van der Werf, K.; Bennink, M.; Subramaniam, V. *Nanoscale Res. Lett.* **2011**, *6*, 270.
(25) Thormann, E.; Pettersson, T.; Claesson, P. M. *Rev. Sci. Instrum.* **2009**, *80*, 093701.
(26) Sader, J. E.; Chon, J. W. M.; Mulvaney, P. *Rev. Sci. Instrum.* **1999**, *70*, 3967.
(27) Green, C. P.; Lioe, H.; Cleveland, J. P.; Proksch, R.; Mulvaney, P.; Sader, J. E. *Rev. Sci. Instrum.* **2004**, *75*, 1988.
(28) Cappella, B.; Dietler, G. *Surf. Sci. Rep.* **1999**, *34*, 1.
(29) Butt, H.-J.; Cappella, B.; Kappl, M. *Surf. Sci. Rep.* **2005**, *59*, 1.
(30) Watanabe, J.; Lepoutre, P. *J. Appl. Polym. Sci.* **1982**, *27*, 4207.
(31) Zang, Y.-H.; Du, J.; Du, Y.; Wu, Z.; Cheng, S.; Liu, Y. *Langmuir* **2010**, *26*, 18331.
(32) Zhang, G.; Wei, Z.; Ferrell, R. E. *Appl. Clay Sci.* **2009**, *43*, 271.
(33) Chen, C.-H.; Kuo, W.-S.; Lai, L.-S. *Food Hydrocolloids* **2010**, *24*, 200.
(34) Husband, J. C.; Gate, L. F.; Norouzi, N.; Blair, D. *Tappi J.* **2009**, *8*, 12.
(35) Chen, B.; Evans, J. R. G. *Carbohydr. Polym.* **2005**, *61*, 455.
(36) Wang, D.-y.; Zhu, Y.-l.; Ma, W.; Niu, Y.-h. *Cold Reg. Sci. Technol.* **2006**, *44*, 12.
(37) Vanorio, T.; Prasad, M.; Nur, A. *Geophys. J. Int.* **2003**, *155*, 319.
(38) Prasad, M.; Kopycinska, M.; Rabe, U.; Arnold, W. *Geophys. Res. Lett.* **2002**, 29.
(39) Johansson, E.; Wågberg, L. *Colloids Surf., A* **2012**, *394*, 14.